



## High-speed friction stir welding in light weight battery trays for the EV industry

Vivek Patel, Jeroen De Backer, Henrik Hindsefelt, Mattias Igestrand, Saeed Azimi, Joel Andersson & Jörgen Säll

To cite this article: Vivek Patel, Jeroen De Backer, Henrik Hindsefelt, Mattias Igestrand, Saeed Azimi, Joel Andersson & Jörgen Säll (2022) High-speed friction stir welding in light weight battery trays for the EV industry, Science and Technology of Welding and Joining, 27:4, 250-255, DOI: [10.1080/13621718.2022.2045121](https://doi.org/10.1080/13621718.2022.2045121)

To link to this article: <https://doi.org/10.1080/13621718.2022.2045121>



© 2022 The Author(s). Published by Informa UK Limited, trading as Taylor & Francis Group



Published online: 01 Mar 2022.



Submit your article to this journal [↗](#)



Article views: 723




View related articles [↗](#)



View Crossmark data [↗](#)

## High-speed friction stir welding in light weight battery trays for the EV industry

Vivek Patel <sup>a</sup>, Jeroen De Backer<sup>a,b</sup>, Henrik Hindsefelt<sup>c</sup>, Mattias Igestrand<sup>a</sup>, Saeed Azimi<sup>d</sup>, Joel Andersson<sup>a</sup> and Jörgen Säll<sup>e</sup>

<sup>a</sup>Department of Engineering Science, University West, Trollhättan, Sweden; <sup>b</sup>Friction Welding Process Section, TWI Ltd., Cambridge, UK; <sup>c</sup>Hydro Extruded Solutions AB, Finspång, Sweden; <sup>d</sup>Volvo Car corporation, Gothenburg, Sweden; <sup>e</sup>ESAB, Laxå, Sweden

### ABSTRACT

Present work aims to achieve high welding speed during friction stir welding of lightweight battery trays in the electric vehicle industry. This study reports high-speed friction stir welding (HSFSW) up to  $4.0 \text{ m min}^{-1}$  in AA6063-T6 alloys. The defect-free HSFSW joints are produced by adopting aggressive material mixing, i.e. higher tool rotation and plunge force. HSFSW weld cross-section reported an unusual hardness profile of 'U' shape instead of 'W' shape in conventional FSW of AA6xxx alloys. HSFSW resulted softening of weld stir zone ( $\sim 60\text{HV}$ ) along with HAZ ( $\sim 53\text{HV}$ ) against the base material (BM) hardness of  $\sim 90\text{HV}$ . The HSFSW at  $4.0 \text{ m min}^{-1}$  obtained good joint strength of 71% of the BM. Microstructure evolutions across the fractured weld cross-section are discussed using EBSD analysis.

### ARTICLE HISTORY

Received 4 December 2021  
Revised 26 January 2022  
Accepted 5 February 2022

### KEYWORDS

High-speed friction stir welding; lightweight; battery trays; electric vehicle; welding speed

### Introduction

The automotive industry is going through the greatest transformation in its existence. The transition from internal combustion engines to zero-emission alternatives such as Battery-electric vehicles (BEV) requires a complete overhaul of design, materials and manufacturing processes. Owing to the low energy density of lithium-ion batteries, compared to fossil fuels, the overall weight of the vehicles is significantly higher. Therefore, light-weighting has become a key priority in other areas of vehicle design. According to the Duckers 2020 report, aluminium usage as a lightweight material is growing at a fast pace. The study forecasts that the weight of the aluminium used in cars is going to increase to 570 pounds by 2030 [1]. The majority of new BEVs adopt a so-called skateboard design, whereby the battery pack is mounted in a (tray) enclosure at the bottom of the car. Often, these trays are fabricated using a combination of extruded, cast and rolled aluminium products. To guarantee the safety for passengers, the trays must be water-tight, impact resistant and stiff, while being fabricated at high production volumes. These high requirements have forced manufacturers to adopt new joining processes such as friction stir welding (FSW).

Friction stir welding is well-suited as a solid-state and sustainable manufacturing technology. FSW has advanced into a mature process for welding of aluminium alloys, and significant literature is available on topics such as evaluations of microstructure and

properties, heat generation, material flow, and process parameters optimisation [2]. Ma et al. [3] presented a dedicated review on the FSW of aluminium alloys by summarising microstructure evolution and mechanical properties in aluminium joints. As far as dissimilar aluminium joints are concerned, the literature on FSW of various dissimilar combinations of aluminium alloys is also documented [4]. Recently, a comprehensive review on microstructure development in various similar and dissimilar material joints are published [5]. Despite of the extensive research on the FSW process, one of the key factors that restricts the implementation of this technology in volume-based production line is relatively low welding speeds, typically around  $0.5\text{--}1.5 \text{ m min}^{-1}$ . However, advancement in FSW tool materials and geometry lead further increase in the welding speed to establish high-speed friction stir welding (HSFSW). In early research, Rodrigues et al. [6] coined the term HSFSW and they demonstrated HSFSW around  $1 \text{ m min}^{-1}$  in AA5083-H111 (4 and 6 mm thickness) and AA6082-T6 (3 and 6 mm thickness) aluminium alloys. They concluded that HSFSW tool parameters are strongly dependent on the base materials characteristics and plate thickness. Bernard et al. [7] and Liu et al. [8] demonstrated HSFSW at  $1.5 \text{ m min}^{-1}$  for AA 5182-H111 (5.15 mm thick) and AA6061-T6 (0.8 mm thick) alloy respectively, and they obtained joint strength near to respective base metals. Naumov et al. [9] exhibited further increase in the welding speed to  $2.5 \text{ m min}^{-1}$  for AA6082-T6 (2 mm thick)

alloy, reporting this HSFSW fractured from the stir zone (SZ), whereas low-speed FSW joint fractured from the heat-affected zone (HAZ). Later, Hovanski et al. [10] achieved HSFSW at  $3.0 \text{ m min}^{-1}$  in AA5182-O (1.2 and 2.0 mm thicknesses) to produce tailor-welded blanks. Similarly, Zhang et al. [11] achieved HSFSW at  $3.0 \text{ m min}^{-1}$  in high strength AA7075-T6 (2 mm thick) by varying tool rotational speed. Also, Liu et al. [12] obtained defect-free joint at  $2.4 \text{ m min}^{-1}$  in HSFSW of AA6005A-T6 (4 mm thick) alloy. In the overall summary of the above HSFSW literature, it has been proven that HSFSW joints result in narrowed down of the softened region followed by reduction in microhardness in the HAZ.

The present study is aimed to increase the welding speed beyond  $3 \text{ m min}^{-1}$  in order to achieve a higher production volume for producing light weight crash-resistant battery tray for EV. In this study, a high welding speed of  $4 \text{ m min}^{-1}$  were produced in the AA6063-T6 alloy butt joint (3 mm thick). Through tool design and weld procedure development. Fully consolidated welds with good mechanical performance were obtained, and a correlation between the microstructure and mechanical property was established.

## Materials and method

Extruded AA6063-T6 aluminium sheets in 3 mm thickness (provided Hydro Extrusions AB) were welded in butt joint configuration. Before the welding, extruded plates were machined to the length of 300 mm and the width of 150 mm. A conventional FSW tool with convex shoulder (convex radius of 60 mm) of 12 mm outer diameter and scroll features (2 spirals with 4 mm pitch) on it was used. The probe had a tri-flat conical shape with a diameter of 6 mm at the root, 4.3 mm at tip, and a pin length of 2.8 mm. The HSFSW was conducted at three different high welding speed of 3.0, 3.5, and  $4.0 \text{ m min}^{-1}$  under a constant rotational speed of  $4500 \text{ rev min}^{-1}$  and the axial downward force of 8.5 kN. The HSFSW experiments were performed on gantry FSW system at Hydro Extruded Solutions AB, Finspång. After HSFSW, the cross-section of welds was prepared for optical microscopy (OM) by grinding and polishing to a  $1 \mu\text{m}$  finish, followed by Keller's reagent etching. Micro-hardness distributions across the weld cross section were acquired using a Struers automated Vickers hardness tester, with a loading condition of 0.2 kg for 10 s at a distance of 0.3 mm. For each weld, three tensile specimens were cut by waterjet cutting in accordance with ASTM E8 sub-size specimen, following the room temperature tensile testing at a constant crosshead speed of  $1 \text{ mm min}^{-1}$  (position controlled) on a Zwick Roell tensile testing machine. Fracture locations were observed by OM, followed by Electron backscattered diffraction (EBSD). To obtain

orientation maps and grain size distributions in fractured weld cross section produced at  $4 \text{ m min}^{-1}$  welding speed, EBSD was carried out with a step size of  $0.5 \mu\text{m}$ . EBSD specimen prepared by electro polishing (20 V) in the solution of 10% perchloric acid in ethanol to generate strain-free surface. The obtained results were analysed using CHANNEL 5, Oxford Instruments HKL software. Grain size measurements were conducted using the linear intercept method. Low and high angle grain boundaries were separated by using the  $10^\circ$  criterion.

## Results and discussion

It was found that HSFSW was highly susceptible to probe failure due to a large amount of axial as well as transverse forces acting onto the probe during high traverse speed. In order to avoid tool breakage, the radial forces (i.e. the combined traverse and side force) during HSFSW could be minimised by increasing the tool rotational speed. So, HSFSW experiments began from very high rotational speed under constant downward axial force required (8.5 kN) for defect-free weld surface as well as cross-section. The important reason behind selecting such a high rotational speed is to ensure the least amount of traverse forces on the tool and avoiding tool fracture during process development. The weld cross sections of HSFSW produced at three welding speeds are shown in Figure 1. As it can be seen from the macrographs, appropriate material mixing across the weld thickness is observed in all three welds. The irregular top surface of the weld cross section is attributed to the scroll feature of tool shoulder. The weld cross section represents a typical microstructural zone of FSW, i.e. stir zone (SZ), thermo-mechanically affected zone (TMAZ), and heat-affected zone (HAZ). The typical basin-shaped SZ with sharper advancing side (AS) interface developed in all three weld cross sections. The joint line remnant is visible as a discontinuous zigzag line through the SZ, as shown in Figure 1. This joint line remnant is formed due to the breaking of initial butt surfaces by the tool during stirring and mixing [9,13]. As it is clear from the macrographs, the remnant joint line becomes more prominent as welding speed increases above  $3.0 \text{ m min}^{-1}$ .

Owing to the fine grain structure in the SZ, grain boundary strengthening along with precipitate strengthening result in stronger SZ. However, the effect of precipitation hardening is weak due to the very high rotational speed in all three HSFSW joints. Hence, different microstructural zones, i.e. SZ, TMAZ, and HAZ develop softening region, and the lowest hardness value usually occurs either in HAZ or TMAZ/HAZ interface. In order to understand softening effect, the microhardness distribution across the weld cross-section of HSFSW joints is shown in Figure 2. The hardness reduction of 35% is found in the SZ of all three weld

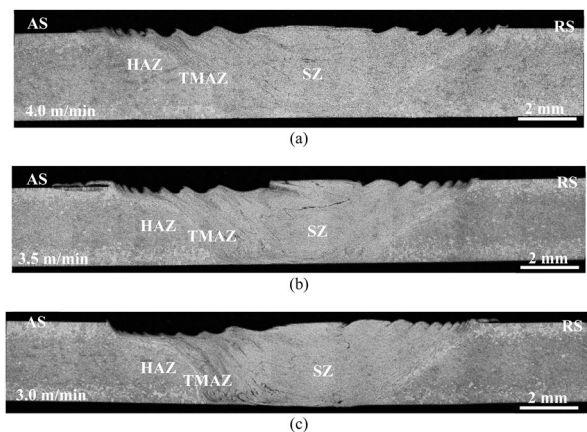


**Figure 1.** Optical micrograph of the weld cross sections at different high welding speeds: (a)  $4.0 \text{ m min}^{-1}$ , (b)  $3.5 \text{ m min}^{-1}$ , and (c)  $3.0 \text{ m min}^{-1}$ .

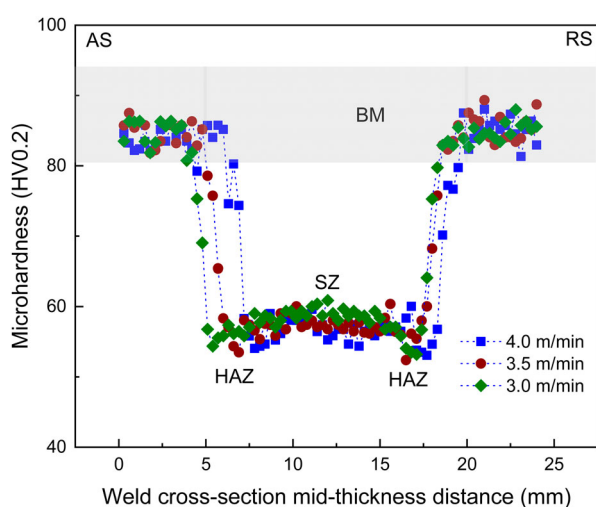


**Figure 2.** Hardness distribution along the mid-thickness of weld cross-section at different welding speeds.

joints. For all three joints, the hardness distribution in SZ is achieved in a mostly uniform manner within 55–60 HV. No significant variation in hardness on AS and RS was measured. The lowest hardness value around  $\sim 53$  HV is obtained at HAZ for all three HSFSW joints. It is worth to note that hardness profile is ‘U-shaped’ for welding speeds more than  $3.0 \text{ m min}^{-1}$ , unlike the typical ‘W-shaped’ distribution in conventional low-speed FSW joints. Moreover, the width of the softened region increases as welding speed decreases. For understanding the strength of these HSFSW joints, tensile testing analysis is presented in Figure 3. The ultimate tensile strength (UTS) of the joints increases as the welding speed increases from 3 to  $4 \text{ m min}^{-1}$ . The difference in UTS is relatively small between joints produced at 4 and  $3.5 \text{ m min}^{-1}$  welding speed, whereas the difference gets more at  $3.0 \text{ m min}^{-1}$  welding speed (refer Table 1).

The highest joint efficiency of 71% reported by joint produced at  $4 \text{ m min}^{-1}$ . To find out the exact failure location, cross-section of tensile tested specimens is

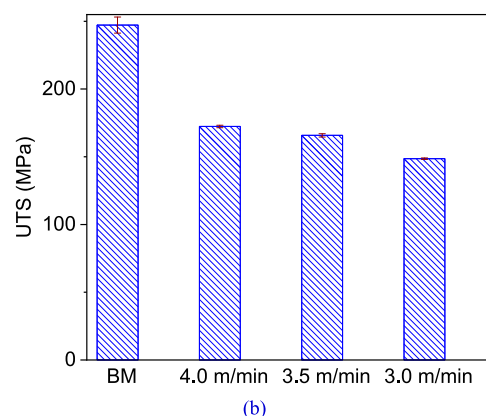
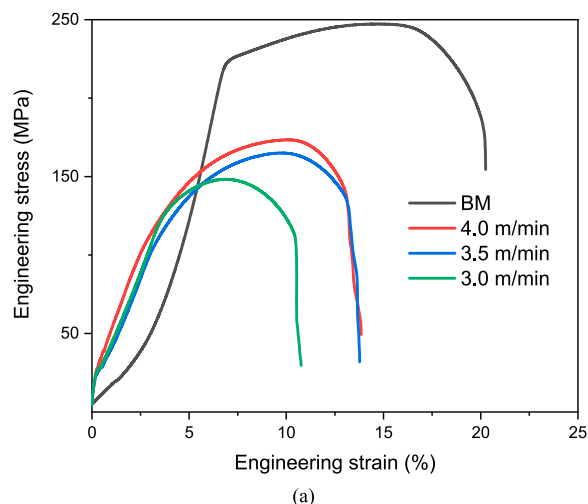


**Figure 3.** Tensile behaviour: (a) stress-strain curve and (b) comparison of tensile properties at different welding speeds along with BM.

**Table 1.** Summary of joint strength and failure location at different welding speeds.

Welding speed ( $\text{m min}^{-1}$ )	UTS (MPa)	Joint efficiency (%)	Failure location
4.0	$174 \pm 0.92$	71	HAZ on RS
3.5	$167 \pm 1.21$	68	HAZ on AS
3.0	$150 \pm 0.54$	61	HAZ on AS

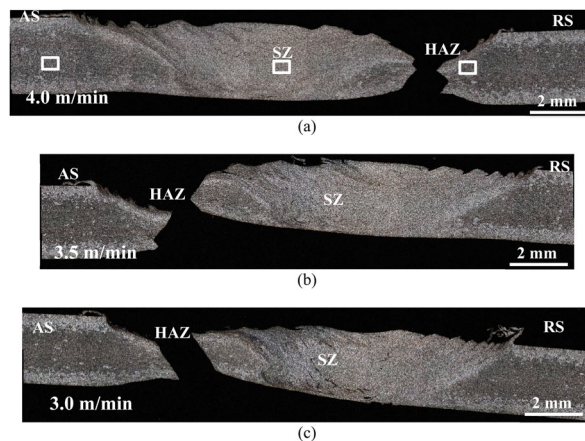


**Figure 4.** Optical micrograph representing fracture location of the weld produced at different welding speeds: (a)  $4.0 \text{ m min}^{-1}$ , (b)  $3.5 \text{ m min}^{-1}$ , and (c)  $3.0 \text{ m min}^{-1}$ .



examined under an optical microscope as shown in Figure 4. As it is clearly seen from the figure, the failure in all HSFSW joints found at HAZ/TMAZ interface. It is worth to note that the tensile strength of the HSFSW joints are not dependent on the presence of remnant of oxide lines in the SZ, since none of the HSFSW joints failed from the SZ during tensile testing. In contradictory, a previous study of HSFSW at  $2.5 \text{ m min}^{-1}$  reported weld failure from SZ itself due to insufficient material mixing, resulting in a weakness along the joint line remnant [9]. In the present study, despite a very high welding speed of  $4 \text{ m min}^{-1}$ , the

weld failure is located outside the SZ, showing adequate material mixing at such a higher rotational speed. The lowest hardness value (refer to Figure 2) in HAZ could be one of the main reasons for the failure location in all HSFSW joints. However, the location of failure changes from AS to RS when welding is increased from  $3.5$  to  $4.0 \text{ m min}^{-1}$ . Furthermore, it can be concluded that the failure is located in the region where the weld is the thinnest, which initiates stress raiser from that rough surface as clearly evident from those higher magnification weld cross-section micrographs in Figure 1. It is important to note that surface preparation of

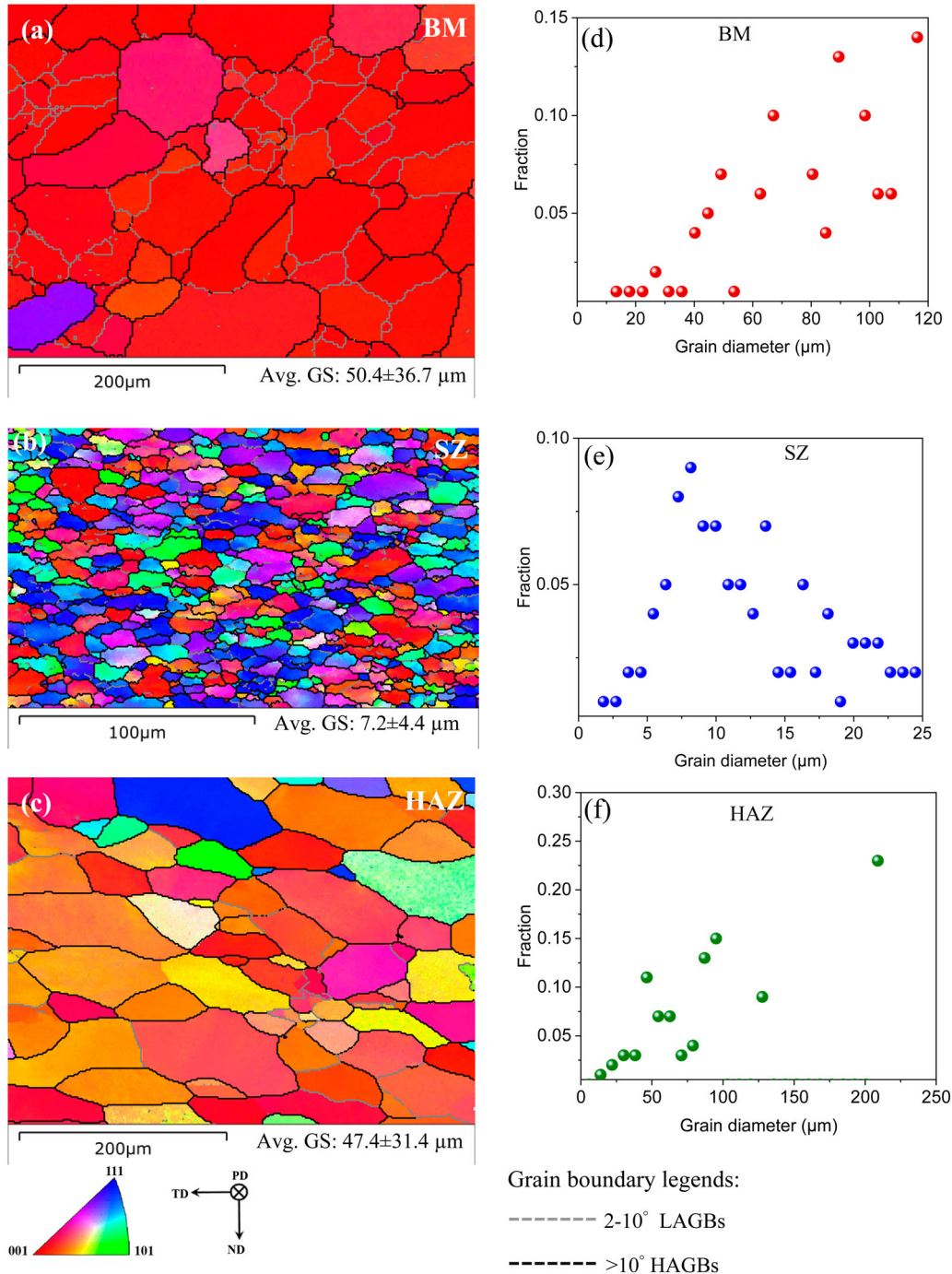


**Figure 5.** EBSD of the different microstructural zones of fractured weld cross section of  $4 \text{ m min}^{-1}$ : Crystallographic orientation maps (a) BM, (b) SZ, (c) HAZ; and grain size distribution of corresponding maps (d) BM, (e) SZ, (f) HAZ corresponding grain size distribution. Note: EBSD location of the different zones are marked with a small rectangle in Figure 4(a).

the tensile specimens was not performed prior to tensile testing. The reason behind this was to evaluate the weld joints strength in as-welded conditions. The tensile specimens are sensitive to thickness variation, and sample at  $3.0 \text{ m min}^{-1}$  has lower thickness near TMAZ/HAZ on AS compared to other portions (refer to Figure 1), thus tensile failure is occurred from this thin region as shown in Figure 4. In order to understand the tensile failure deformation in the highest joint strength sample ( $4.0 \text{ m min}^{-1}$ ), EBSD analysis of the distinguished microstructural zones, i.e. SZ, HAZ and BM were conducted as location marked with a small rectangle in Figure 4(a). Figure 5 presents crystallographic orientation maps representing high angle grain boundaries (HAGBs) and low angle grain boundaries (LAGBs) along with grain size distribution of fractures weld cross section of  $4.0 \text{ m min}^{-1}$  welding speed. As shown in Figure 5(a–c), the SZ represents fine equiaxed grain refinement of  $7.2 \mu\text{m}$  from the coarse grain size of  $\sim 50 \mu\text{m}$  of BM. EBSD analysis found that HSFSW microstructural zones, i.e. SZ and HAZ are similar to conventional low welding speed FSW. The fine grains in SZ are resulted due to the occurrence of tensile deformation. This grain refinement in SZ is due to the

severe plastic deformation occurred by a combination of aggressive rotational and welding speed. However, hardness distribution in HSFSW found different from the conventional low welding speed FSW. In HSFSW, despite the significant grain refinement in the SZ, the hardness variation between SZ and HAZ was found to be minimal, unlike low welding speed FSW [12]. So, to achieve high welding speed, the use of higher rotational speed and plunge force nullifies the effect of grain refinement on hardness improvement in the SZ. The lowest hardness zone, i.e. HAZ presented a coarse grain size of  $\sim 47 \mu\text{m}$  near that of the BM. The distribution of the grain boundaries misorientation of the microstructural zones is displayed in Figure 6. During tensile deformation, different crystal orientation between HAZ and BM along with more HAGBs of 80% in HAZ as compared to HAGBs of 56% in BM. The SZ grain boundaries are characterised by more fraction of HAGBs (86%), enhancing in tensile deformation of the joint. Moreover, grain size distribution is found in a uniform manner where a large fraction of the grains measured below  $10 \mu\text{m}$ , as presented in Figure 5(e). In summary, our initial goal of achieving  $4 \text{ m min}^{-1}$  in HSFSW has resulted in good joint strength.

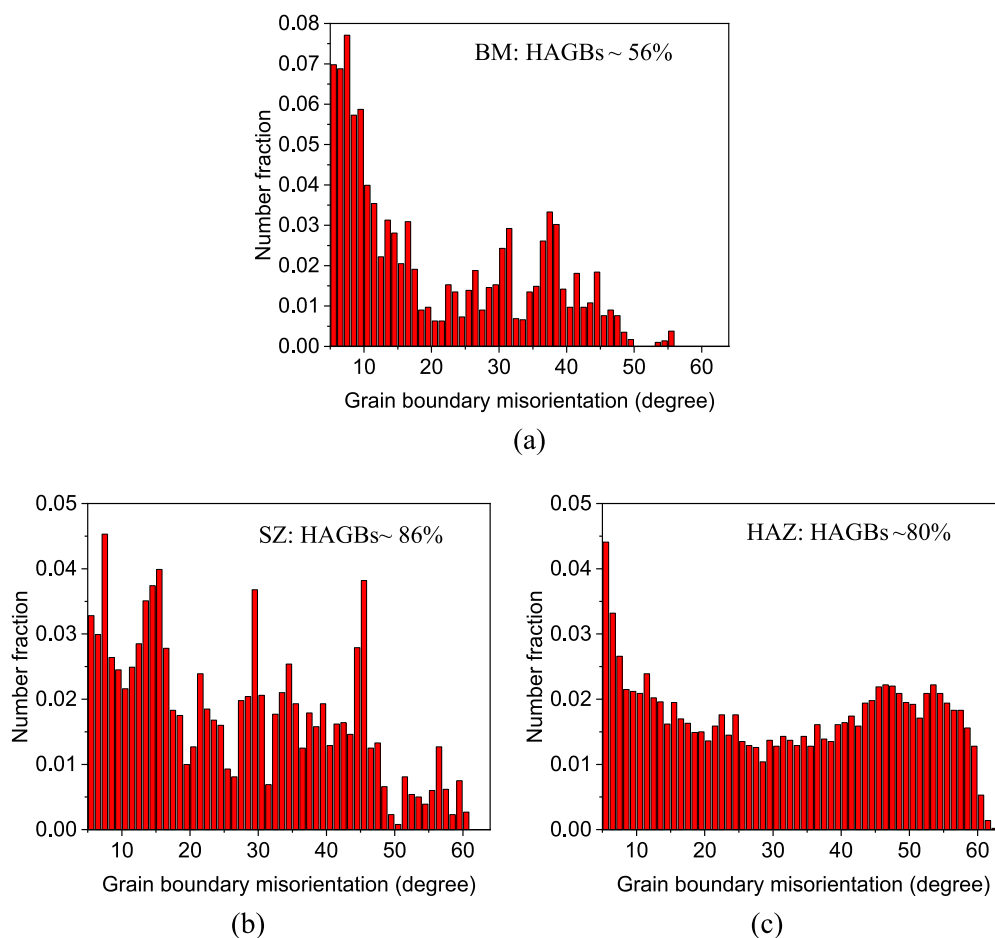


**Figure 6.** Grain boundaries misorientation histograms in the different weld zones produced at  $4.0 \text{ m min}^{-1}$  welding speed: (a) BM, (b) SZ, (c) HAZ.

## Conclusions

In the present study, defect-free HSFSW of 3 mm thick AA6063-T6 alloys in BEVs was achieved at a welding speed of  $4.0 \text{ m min}^{-1}$ . All HSFSW joints were developed without any defects and tool failure. The wider weld cross-section at all the welding speeds exhibits the combination of large probe diameter and rotational speed. EBSD analysis in the different microstructure zone confirmed the significant grain refinement in the SZ along with a large fraction of HAGB, which resulted in tensile deformation. The HSFSW joint produced at  $4.0 \text{ m min}^{-1}$  achieved 71% of joint strength, exhibiting tensile failure from the TMAZ/HAZ interface, coinciding with the location of lowest hardness, i.e. 53 HV. The development of this HSFSW at  $4.0 \text{ m min}^{-1}$  is expected to scale up as well as strengthen the production of lightweight battery tray for EVs. Moreover, the results of this study will help to further increase the welding speed beyond  $4 \text{ m min}^{-1}$  by improving the weld surface.

## Disclosure statement

No potential conflict of interest was reported by the author(s).

## Funding

The authors acknowledge the funding support from the Swedish funding body VINNOVA under the project of EVA-STIR (2019-03114) and industry partners Volvo Car Corporation, Hydro Extruded Solutions, and ESAB.

## ORCID

Vivek Patel  <http://orcid.org/0000-0002-9015-7372>

## References

- [1] DuckerFrontier North American Light Vehicle Aluminum Content and Outlook Drive Aluminum. [cited 2021 Mar 27]. Available from: <https://www.drivealuminum.org/research-resources/duckerfrontier-north-american-light-vehicle-aluminum-content-and-outlook-august-2020>.

- [2] Padhy GK, Wu CS, Gao S. Friction stir based welding and processing technologies – processes, parameters, microstructures and applications: a review. *J Mater Sci Technol*. 2018;34(1):1–38.
- [3] Ma ZY, Feng AH, Chen DL, et al. Recent advances in friction stir welding/processing of aluminum alloys: microstructural evolution and mechanical properties. *Crit Rev Solid State Mater Sci*. 2018;43(4):269–333.
- [4] Patel V, Li WY, Wang G, et al. Friction stir welding of dissimilar aluminum alloy combinations: state-of-the-art. *Metals (Basel)*. 2019;9(3):270.
- [5] Heidarzadeh A, Mironov S, Kaibyshev R, et al. Friction stir welding/processing of metals and alloys: a comprehensive review on microstructural evolution. *Prog Mater Sci*. 2021;117: 100752.
- [6] Rodrigues DM, Leitão C, Louro R, et al. High speed friction stir welding of aluminium alloys. *Sci Technol Weld Joining*. 2010;15(8):676–681.
- [7] Bernard D, Hattingh DG, Goosen WE, et al. High speed friction stir welding of 5182-H111 alloy: temperature and microstructural insights into deformation mechanisms. *Met Mater Int*. 2021;27(8):2821–2836.
- [8] Liu F, Fu L, Chen H. High speed friction stir welding of ultra-thin AA6061-T6 sheets using different backing plates. *J Manuf Process*. 2018;33:219–227.
- [9] Naumov A, Morozova I, Rylkov E, et al. Metallurgical and mechanical characterization of high-speed friction stir welded AA 6082-T6 aluminum alloy. *Materials (Basel, Switzerland)*. 2019;12(24):4211.
- [10] Hovanski Y, Upadhyay P, Carsley J, et al. High-speed friction-stir welding to enable aluminum tailor-welded blanks. *JOM*. 2015;67(5):1045–1053.
- [11] Zhang J, Upadhyay P, Hovanski Y, et al. High-speed friction stir welding of AA7075-T6 sheet: microstructure, mechanical properties, micro-texture, and thermal history. *MMTA*. 2018;49(1):210–222.
- [12] Liu H, Liu X, Wang X, et al. Mechanical properties and their relations to microstructural characteristics of high-speed friction stir-welded AA6005A-T6 aluminum hollow extrusions. *Int J Adv Manuf Technol*. 2017;88(9):3139–3149.
- [13] Niu P, Li W, Zhang Z, et al. Significant effect of oxide on mechanical properties of friction-stir-welded AA2024 joints. *Sci Technol Weld Joining*. 2017;22(1):66–70.